http://www.jstage.jst.go.jp/browse/biophysics

BIOPHYSICS

REVIEW

Vol. 9, pp. 141–148 (2013)
doi: 10.2142/biophysics.9.141

3D structure of eukaryotic flagella/cilia by cryo-electron tomography

Takashi Ishikawa[1]

[1]*Laboratory of Biomolecular Research, Paul Scherrer Institute, Villigen PSI, CH5232, Switzerland*

Received July 9, 2013; accepted September 25, 2013

Flagella/cilia are motile organelles with more than 400 proteins. To understand the mechanism of such complex systems, we need methods to describe molecular arrangements and conformations three-dimensionally in vivo. Cryo-electron tomography enabled us such a 3D structural analysis. Our group has been working on 3D structure of flagella/cilia using this method and revealed highly ordered and beautifully organized molecular arrangement. 3D structure gave us insights into the mechanism to generate bending motion with well defined waveforms. In this review, I summarize our recent structural studies on flagella/cilia by cryo-electron tomography, mainly focusing on dynein microtubule-based ATPase motor proteins and the radial spoke, a regulatory protein complex.

Key words: dynein, microtubule, cryo-EM, axoneme, motor protein

Introduction – flagella/cilia

Flagella and motile cilia in eukaryotes are bending organelles, which generate cellular motility (Fig. 1a) or flow of extracellular fluid. In most of the eukaryotes, they share a common "9+2" structure (Fig. 1b): two singlet microtubules are surrounded by nine microtubule doublets (MTDs) (grey in Fig. 1b and Fig. 2a). Although there are other types of flagella/cilia, non-motile primary cilia and "9+0" motile cilia, in this review I cover only the "9+2" structure. Proteomics demonstrated that there are more than 400 proteins in flagella/cilia[1], most of which have not been characterized and located. Between adjacent MTDs there are a number of linkers. The most prominent are dynein motor proteins, which were identified by Gibbons[2]. Dyneins are a family of gigantic ATPase motors with more than 4,500 amino acids with an N-terminal tail and a C-terminal head with six AAA+ motifs, which forms a ring (Fig. 3b)[3]. According to the recently revealed crystal structures[4,5], a coiled-coil stalk extends from AAA4 and there is a microtubule binding domain (MTBD) at the tip of the stalk (Fig. 3). In flagella, dyneins are forming two structures: outer and inner dynein arms (ODA and IDA) (red in Fig. 1b) anchored on one MTD at their N-terminal tails and dynamically interact with another MTD at MTBD. There is another linker (nexin) connecting adjacent MTDs, but its function is unknown. MTDs and the central singlet microtubules are connected by radial spokes (RSs) (light blue in Fig. 1b). This "9+2" structure has been known since 50's[6] by electron microscopy (EM) of plastic embedded cross sections of flagella. In early 80's, EM of longitudinally sectioned and freeze-fracture deep-etched flagella/cilia proved the periodicity[7,8]. ODAs form an array with a 24 nm periodicity, while IDA and RS make a 96 nm periodicity.

Cryo-electron tomography and subtomogram averaging

The microtubule-based power stroke of dynein is supposed to be a driving force of flagellar/ciliary bending. However, both the mechanism of dynein power stroke and the mechanism of bending by integrating individual dyneins were unknown. How do various proteins cooperate together to generate bending motion? How are conformational changes of individual components integrated into a well orchestrated waveform? To address these questions, we need 3D structural

Corresponding author: Takashi Ishikawa, Laboratory of Biomolecular Research, Paul Scherrer Institute, Villigen PSI, CH5232, Switzerland.
e-mail: takashi.ishikawa@psi.ch

©2013 THE BIOPHYSICAL SOCIETY OF JAPAN

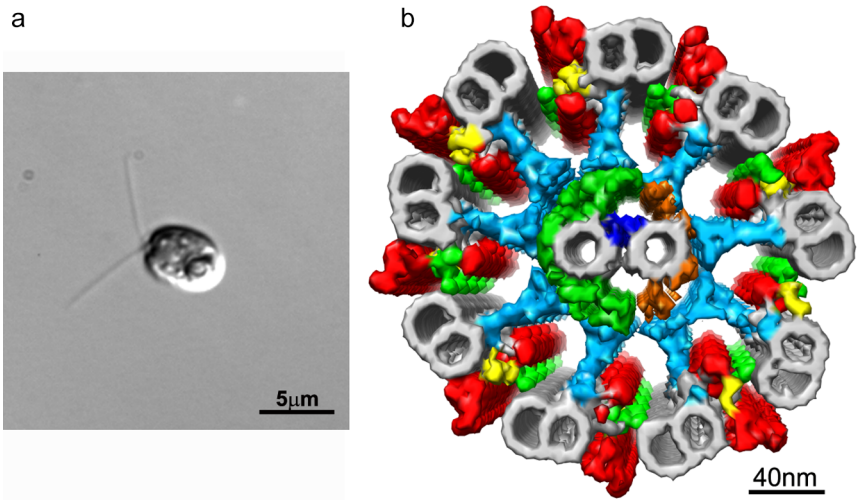

Figure 1 Flagella/cilia from eukaryotes. (a) Differential interference contrast micrograph of green algae *Chlamydomonas*. Two flagella are seen. (b) 3D structure of *Chlamydomonas* flagellum seen from the tip (distal end) based on our tomography. Grey: microtubule doublets (MTD) and central singlet microtubules. Red: inner and outer dynein arms (IDA and ODA). Light blue: radial spokes (RS). Structures which are not mentioned in this article are as follows. Green: nexin (on MTD) and central sheath (around singlet microtubules). Yellow: intermediate and light chains of dynein f. Orange: central sheath.

analysis of molecules in vivo, i.e. in flagella/cilia instead of as extracted in vitro. Recently developed cryo-electron tomography technique[9] is suitable method for such a study.

In cryo-electron tomography transmission electron micrographs are recorded from specimen embedded in amorphous ice and tilted in the stage of the microscope. The maximum thickness of the specimen is limited at ~1 μm or ~0.5 μm at the accelerating voltage of 300 kV or 200 kV, respectively. In fact flagella/cilia are suitable target for cryo-EM, since their thickness is ~0.3 μm and isolated flagella/cilia keep bending function. Since the tomographic acquisition requires multiple illumination (in our case, we illuminated one specimen 61 times – from −60 degrees to 60 degrees with 2 degrees of increment), the resolution is limited by radiation damage, up to ~30 Å resolution.

Due to the poor contrast between proteins and amorphous ice under extremely low dose (~0.5e^-/Å^2 for each image), we must improve signal-to-noise ratio by averaging volumes extracted from tomograms, which suppose to have identical structure. Such a volume is called a subtomogram. 96 nm periodicity along MTD and pseudo-nine-fold arrangement of nine MTDs enable us to average more than 1000 subtomograms extracted from ~20 tomograms. However, subtomograms extracted along MTDs, which are not perfectly straight, must be aligned. The alignment is not possible by simple cross-correlation, due to poor signal-to-noise ratio and missing information from limited tilt angles for tomographic data acquisition. Furthermore, in the presence of nucleotides we found heterogeneity in the conformation of dyneins. To deal with structural heterogeneity we developed a method to classify subtomograms based on 3D image analysis. The detail of our subtomogram alignment, classification and averaging are described elsewhere[10].

Overall structure of flagella/cilia

After subtomogram averaging from tomograms of *Chlamydomonas* flagella (Fig. 2a), we found three large densities stacking vertically (i.e. perpendicular to MTD) with 24 nm periodicity (light blue in Fig. 2a) and eight along the MTD (red in Fig. 2a). These densities have a ring shape and 12–15 nm diameter, indicative of dynein heads. Indeed when we analyzed mutant lacking dynein isoforms some densities were missing in the density map. By comparing 3D structure of such mutant flagella, we identified dynein isoforms in the averaged subtomograms (Fig. 2b)[11]. This basic structure is shared by other species such as sea urchin sperms[12,13], *Tetrahymena*[13] and mouse respiratory cilia[14], except the number of dyneins in ODA.

Our structure gave insight into the conformation and arrangement of outer and inner dyneins. Each dynein molecule consists of a long N-terminal tail, a linker and the head with six AAA+ domains. All the eleven (three outer and eight inner) dyneins extend the N-termini (black dotted lines in Fig. 3a,b,c,e) toward the (+) end of the MTD (the distal end of the flagella) and the stalks toward the adjacent MTD with slight tilt to the (−) end of the MTD (the proximal end of the flagella) (yellow in Fig. 3d,e). This basic conformation is common among all the axonemal dynein in our average. Variation was found in the heads of inner arm dyneins. In principle, they are parallel to the surface of MTD, similarly to outer arm dyneins. However, the angles of the heads have variation of ~30 degrees (Fig. 2a). Further variation appears in the conformation of the N-terminal tails (Fig. 2b). Conformation of the N-terminus and the angle of the head might be linked to each other and cause such specific performances of dynein isoforms as velocity, torque and duty ratio[15].

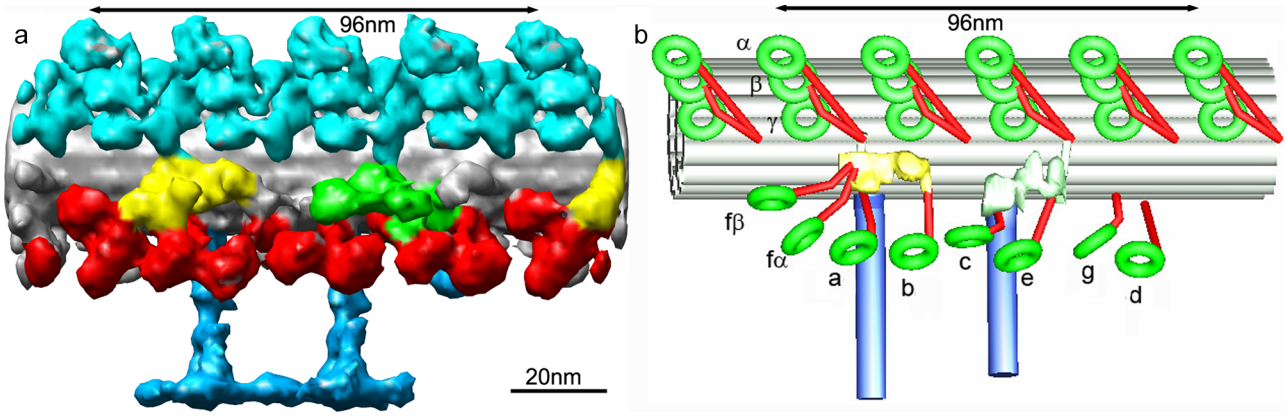

Figure 2 Molecular arrangement on MTD. (a) Averaged subtomograms to cover a 96 nm periodic unit. Grey: MTD. Light blue: ODA. Red: IDA. Blue: RS. Green: nexin. Yellow: Light and intermediated chain of dynein f. (b) Diagram of dyneins based on (a) and 3D analysis of mutants. Green: ATPase rings. Red: N-terminal tails. Dynein isoforms are indicated. Proximal and distal ends are left and right, respectively.

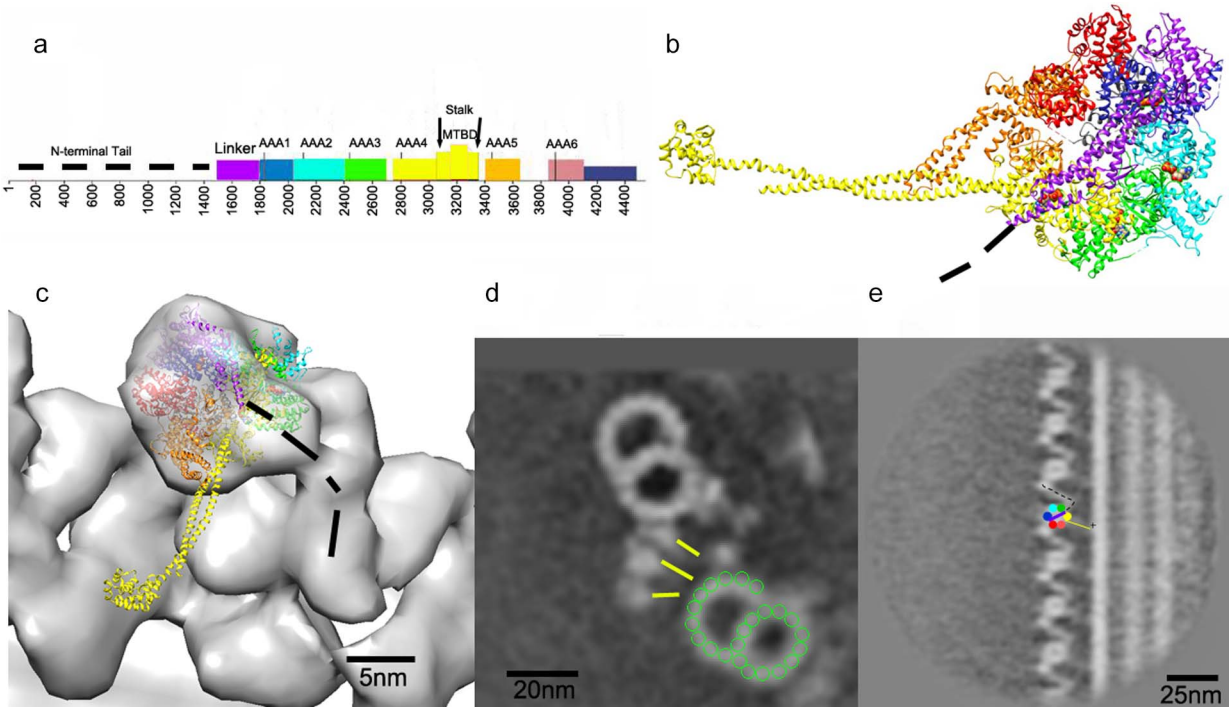

Figure 3 Dynein. (a) Sequence of dynein. Six AAA+ domains are indicated by color. The N-terminal tail is shown as a dotted line. (b) Atomic model of a dynein head (PDB ID: 3VKH). Six AAA+ domains form a ring. (c) The atomic model was fitted to our averaged tomogram. (d) Cross section and (e) longitudinal section of the averaged map. In (d)(e) six AAA+ domains are shown in the same color code as (b) and (c). The stalk is shown as yellow lines. In (c), the proximal and the distal ends are left and right, respectively.

Circumferential and longitudinal asymmetry of inner arm dyneins

Many flagella/cilia have asymmetric waveforms. *Chlamydomonas* flagella, under the low calcium condition, move in a planar asymmetric waveform like breast-stroke. *Tetrahymena* cilia takes a similar planar asymmetric waveform. There should be structural mechanism to generate asymmetric and planar waveforms. By careful analysis, we revealed that the apparent structural symmetry is broken in *Chlamydomonas* flagella[16,17]. Asymmetry exists both among nine MTDs (circumferential asymmetry) and between the proximal and central/distal regions (longitudinal asymmetry).

Some asymmetric molecular arrangements have been known since the lack of ODA in one MTD (called MTD1) which are apposed between two flagella of *Chlamydomonas* as well as connections between MTD1 and MTD2 localized at the proximal region were reported[18]. However, the asym-

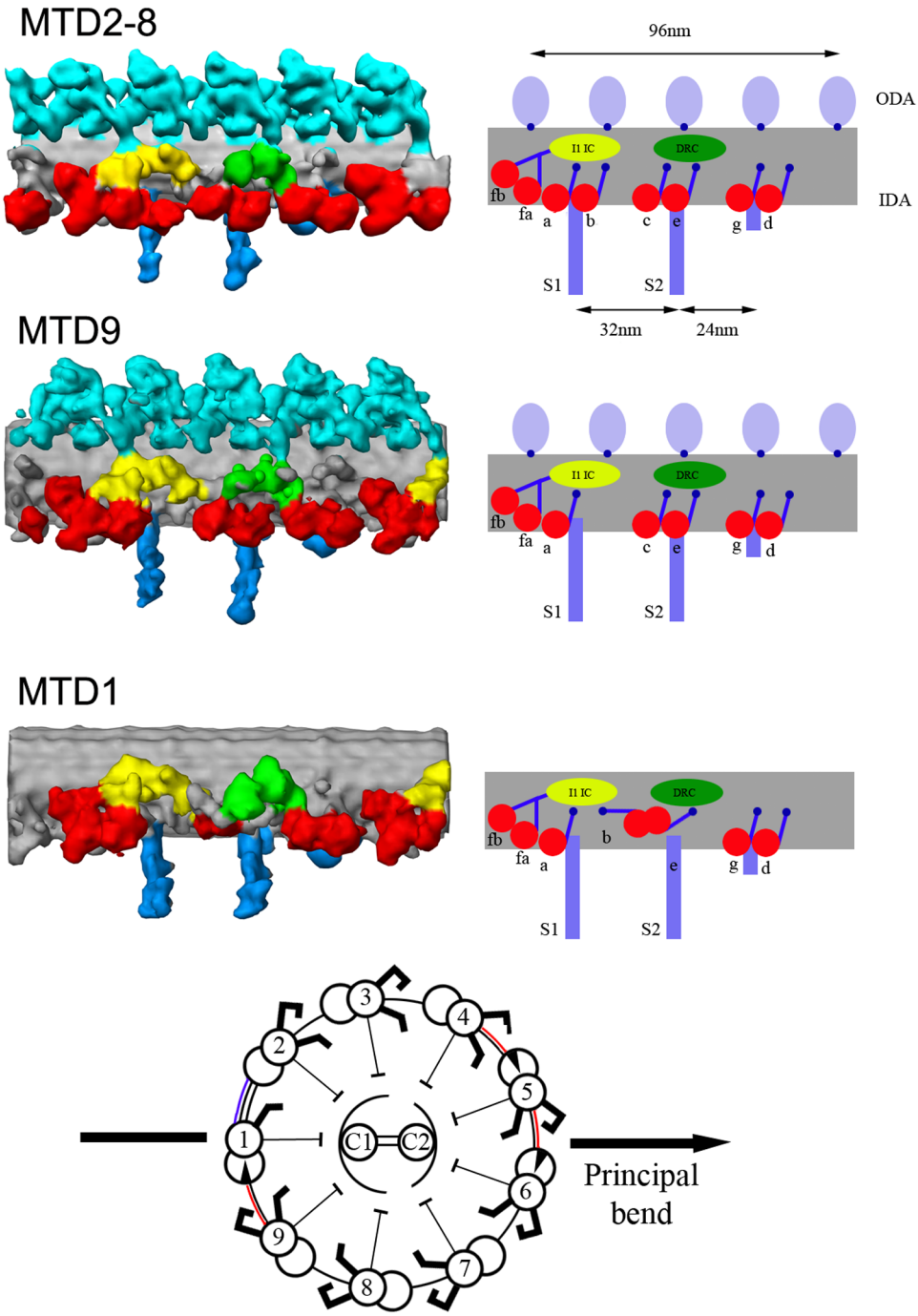

Figure 4 Circumferential asymmetry of IDA arrangement. Left: averaged subtomograms from nine MTDs of *Chlamydomonas* flagella. The numbering of MTDs is shown in the bottom panel. The color code is the same as Figure 2a. Right: schematic diagram of inner arm dyneins based on the left panels. In the six top panels, the proximal and distal ends are at left and at right, respectively. In the bottom panel, the positions of IDL2 and IDL3 are shown in red and purple lines, respectively. Modified from ref. 16.

metry of ODA cannot explain the asymmetric waveform, because the oda1 mutant, which lacks the entire ODA and thus has no asymmetry of ODA, keeps the intact asymmetric waveform[19,20]. We extracted subtomograms from individual MTDs separately and averaged them[16]. This analysis uncovered the asymmetry of IDA and other linkers between adjacent MTDs. In MTD9, dynein b is missing (Fig. 4), while seven MTDs (MTD2 to MTD8) bind all the eight dyneins in IDA. MTD1 lacks not only ODAs but also some IDAs (they might exist and be misfolded, judging from the density close to the surface of MTD in Fig. 4). This result indicates fewer dyneins, therefore less sliding force, at the internal

side (corresponding to MTDs9, 1, 2) of the two flagella of *Chlamydomonas*, which could lead to the asymmetric waveform. We found another density between MTDs arranged in the asymmetric way. One linker (we call them interdoublet linker 2 (IDL2)) exists only between MTD9 and MTD1, and between MTD4, MTD5 and MTD6. The other linker (IDL3) connects only between MTD1 and MTD2. These linkers exist only along the bending plane. They could restrict the sliding between MTD9, 1, 2, 4, 5 and 6. Weaker sliding at these MTDs and stronger sliding at the other MTDs located distantly from the plane would limit the flagellar motion in the plane.

In *Chlamydomonas*, there are 16 dynein genes. One is cytoplasmic dynein, while three are outer arm dyneins. There should be 12 inner dyneins, whereas only eight were purified biochemically[21] and structurally[11] identified. The other unidentified four dyneins were called minor dyneins. Newly developed antibodies of the minor dyneins and fluorescent microscopy proved that minor dyneins are localized at the proximal (within 2 μm from the basal body) region[22]. By combining 3D reconstruction of WT and mutants specifically at the proximal region, we proved that minor dyneins are replacing the other (major) dyneins at the proximal region[17]. This indicates modulated sliding at the proximal region. Further characterization of the minor dyneins is awaited.

Conformational change of dyneins induced by nucleotide hydrolysis and cluster of dynein conformational changes

To structurally characterize power stroke mechanism of dynein we reconstructed tomograms of *Chlamydomonas* flagella in the presence of 1 mM ADP and vanadate (ADP.Vi)[23]. Vanadate mimics phosphate in dynein[24,25] and therefore in the presence of ADP.Vi dynein is supposed to be trapped in the ADP.Pi state. We expected that all the dyneins will be trapped in the ADP.Vi conformation, which corresponds to the pre-power stroke state. However, interestingly, we found heterogeneity in both outer and inner arm dyneins in the presence of ADP.Vi[23]. The total average of subtomograms was blurred in the presence of ADP.Vi. We assumed that there coexist at least two structures, one in the apo conformation and another in the ADP.Vi conformation. We classified extracted subtomograms based on the averaged subtomograms from flagella without nucleotides (in the presence of apyrase) and the averaged subtomograms in the presence of 1mM ADP.Vi, as the templates representing the apo and the ADP.Vi forms, respectively. After the initial classification, subtomograms classified into the class of the ADP.Vi form were averaged to generate the new ADP.Vi template. We used this updated template and the same apo template to iterate classification and averaging until the iteration was converged (detail written elsewhere[23]). By this analysis we obtained 3D structure of dyneins in the ADP.Vi form as well as the distribution of the two conformations. Even more interesting is that the two conformations do not appear randomly, but form clusters (Fig. 5a). Seemingly there is a mechanism to generate positive and/or negative feedback between adjacent ODAs (Fig. 5b). Indeed we demonstrated suppressed ATPase activity of dynein in flagella/cilia[26]. While the length and frequency of the clusters varies, the correlation between the pattern of the ODA clusters and flagellar bending (for example, curvature of the flagella or inside/outside of the curved flagella) is still unclear and should be an important topic in the near future.

Classification enabled us to refine the dynein structure in the ADP.Vi form (Fig. 5c). The dynein tail undergoes conformational changes induced by nucleotides. Concomitant to this reconformation, the dynein head moves ~8 nm toward the (–) end (the proximal end of the flagella), when ADP.Vi binds. We also reconstructed the structure of dynein in flagella in the presence of ADP. The dynein structure with ADP is similar to the apo conformation[23]. This suggests the 8 nm shift of the dynein tail end toward the (–) end (the proximal end of the flagella) upon Pi release to generate the sliding between the adjacent MTDs. No rotation of dynein heads was detected (Fig. 5c): the orientation of the stalk emerging from the head is always the same. This result support the "winch" hypothesis, in which the dynein head moves and drags the adjacent MTD, instead of rotating to push the adjacent MTD (the "rotation" hypothesis), which were a long-term debate using in vitro systems[27,28].

Structure of the radial spokes

It is known that flagella change their waveform induced by calcium ions[29]. The radial spoke includes calmodulin and therefore is considered as a key component of the waveform regulation. We reconstructed the 3D structure of the radial spokes, which connect the central singlet microtubules and the peripheral MTDs (Fig. 6). Ultrastructure of radial spokes have been studied using freeze-fracture deep-etch electron microscopy[30] and was depicted as a "T" shape. *Chlamydomonas* flagella have two radial spokes within the 96 nm periodic unit, while *Tetrahymena* cilia have three. Although this has been known since 80's, we still do not know the mechanism to cause this difference and the meaning in the context of motility of these two organisms. 23 component proteins were identified from *Chlamydomonas* radial spokes (named RSP1–23)[31], while the localization and structure of these proteins are unclear.

Our 3D reconstruction[32] provided more detailed structure, beyond the "T" shape. In addition, by comparing three mutants lacking different components, we located groups of these components[32]. RSP1, 4, 6, 9 and 10 belong to the head region, the interface to the central singlet microtubules, while RSP2, 16 and 23 form the neck region. Interestingly, while other RSPs in the stalk region contain typical signal transduction motifs, the head proteins do not have any par-

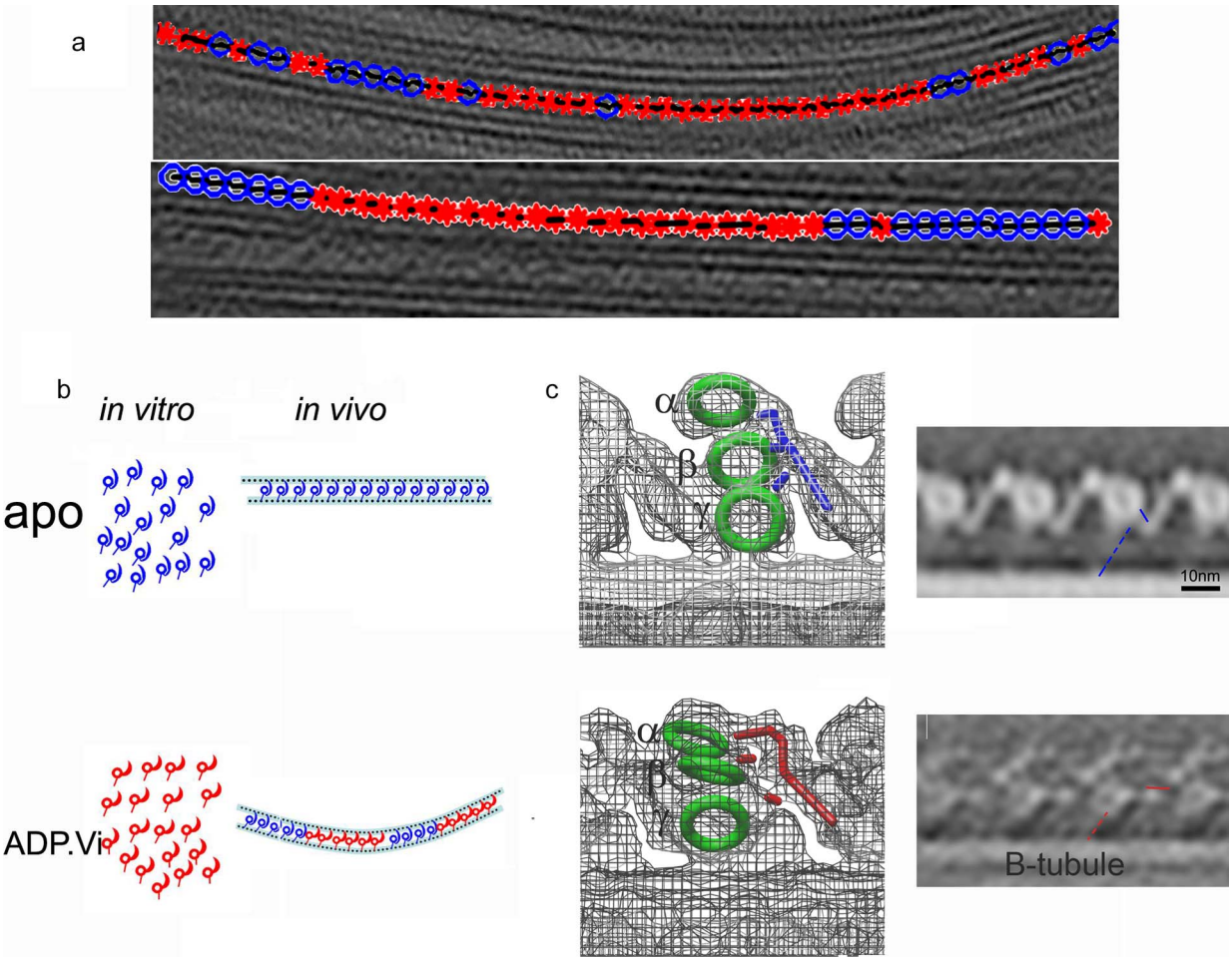

Figure 5 Classification and averaging to find conformational change of dyneins induced by nucleotides. (a) Classification of ODA from two tomograms of flagella in the presence of ADP.Vi. Red: ADP.Vi form. Blue: apo form. (b) Schematic diagram of dynein structural change in vitro and in vivo. (c) Averaged structure of ODA with (bottom) and without (top) ADP.Vi. (left) Wireframe representation with a molecular model fitted. (right) Slices showing the head and the adjacent MTD linked by stalks. The heads are in green. The N-terminal tails are in blue and red. The stalks are indicated by dotted lines. In (c) the proximal and distal ends are at left and at right, respectively. Modified from ref. 23.

ticular motif, except the MORN motif, which is known to be associated with membranes (although no membrane has been found at the interface between the radial spoke and the central singlet microtubules). The radial spoke heads show two-fold symmetry at this resolution (the black ellipsoid in Figure 6c indicate the two-fold axis). Since the central microtubule has a polarity, there should be symmetry mismatch.

Another important finding was on the third radial spoke from *Tetrahymena* cilia (arrow in Fig. 6b). In our 3D reconstruction, the first and the second radial spokes share almost identical structure, while the third spoke demonstrates obvious difference. Interestingly *Chlamydomonas* flagella have a short protrusion at the position of the third spoke of *Tetrahymena*. This short protrusion resembles the bottom part of the third spoke (Fig. 6a), suggesting this protrusion has the same components as the third spoke of *Tetrahymena*. *Chlamydomonas* either stopped its development or degeneration occurred during the evolution. This short protrusion stays intact even all the 23 RSPs are missing in a mutant of *Chlamydomonas*. This fact and distinctive morphology indicate that the third spoke consists of different proteins from the other two spokes.

Outlook

Until now the number of proteins we located by cryo-electron tomography is limited to less than 50. While we have analyzed all the available dynein and radial spoke mutants to locate their components, there are still more than 300 protein components from flagella/cilia to be located and characterized. Since we cannot expect in vivo cryo-EM imaging to reach enough resolution to identify protein sequences, we need systematic labeling or tagging for protein identification.

For further analysis of the conformational change of dy-

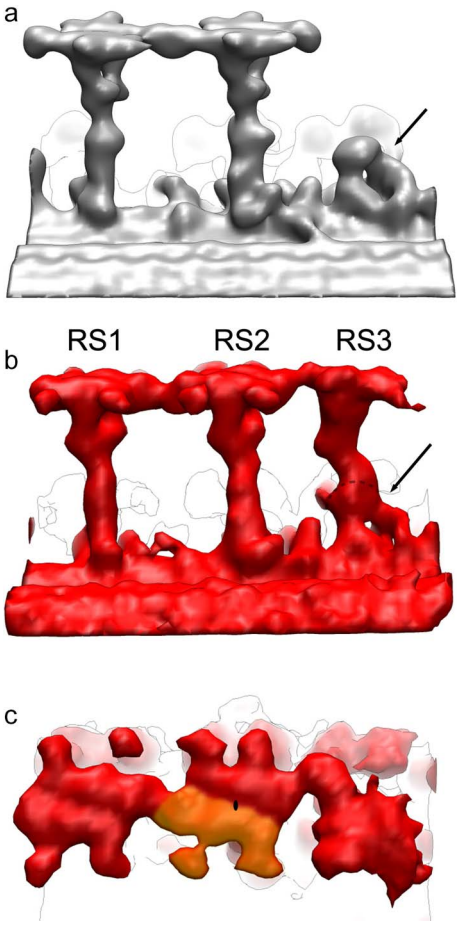

Figure 6 Radial spoke structure. (a) *Chlamydomonas*. (b) *Tetrahymena*. RSs are seen from the adjacent MTD. The third spoke in (b) and the protrusion with similar morphology in (a) are indicated by arrows. (c) *Tetrahymena* RS heads seen from the central singlet microtubule. Left: proximal end. Right: distal end. In (c) the two-fold axis within RS2 is shown by a black ellipsoid. Modified from ref. 32.

neins, we need higher resolution and more sophisticated classification. Recently developed direct electron detectors[33] will help us to obtain data with higher resolution, more contrast and less radiation damage. More computational resource will be required for objective (unsupervised) classification such as the maximum likelihood method[34].

Acknowledgement

These studies described in this review were carried out by Dr. Khanh Huy Bui, Dr. Tandis Movassagh, Dr. Gaia Pigino, Dr. Hironori Ueno and Dr. Aditi Maheshwari. I would also acknowledge our collaborators, Prof. Kazuhiro Oiwa, Dr. Hitoshi Sakakibara (NICT), Prof. Ritsu Kamiya, Prof. Chikako Shingyoji, Dr. Toshiki Yagi, Dr. Ryosuke Yamamoto (Univ. Tokyo) and Prof. Pietro Lupetti (Univ. Siena) and Dr. Dennis Diener (Yale).

References

1. Pazour, G.J., Agrin, N., Leszyk, J. & Witman, G.B. Proteomic analysis of a eukaryotic cilium. *J. Cell Biol.* **170**, 103–113 (2005).
2. Gibbons, I.R. & Rowe, A.J. Dynein: A protein with adenosine triphosphatase activity from Cilia. *Science* **149**, 424–426 (1965).
3. Ishikawa, T. Structural biology of cytoplasmic and axonemal dyneins. *J. Struct. Biol.* **179**, 229–234 (2012).
4. Kon, T., Oyama, T., Shimo-Kon, R., Imamula, K., Shima, T., Sutoh, K. & Kurisu, G. The 2.8 Å crystal structure of the dynein motor domain. *Nature* **484**, 345–350 (2012).
5. Schmidt, H., Gleave, E.S. & Carter, A.P. Insights into dynein motor domain function from a 3.3-Å crystal structure. *Nat. Struct. Mol. Biol.* **19**, 492–497 (2012).
6. Afzelius, B.A. The fine structure of the sea urchin spermatozoa as revealed by the electron microscope. *Z. Zellforsch. Mikrosk. Anat.* **42**, 134–148 (1955).
7. Goodenough, U.W. & Heuser, J.E. Outer and inner dynein arms of cilia and flagella. *Cell* **41**, 341–342 (1985).
8. Mastronarde, D.N., O'Toole, E.T., McDonald, K.L., McIntosh, J.R. & Porter, M.E. Arrangement of inner dynein arms in wild-type and mutant flagella of Chlamydomonas. *J. Cell Biol.* **118**, 1145–1162 (1992).
9. Lučić, V., Leis, A. & Baumeister, W. Cryo-electron tomography of cells: connecting structure and function. *Histochem. Cell Biol.* **130**, 185–196 (2008).
10. Bui, K.H. & Ishikawa, T. 3D structural analysis of flagella/cilia by cryo-electron tomography. *Methods Enzymol.* **524**, 305–323 (2013).
11. Bui, K.H., Sakakibara, H., Movassagh, T., Oiwa, K. & Ishikawa, T. Molecular architecture of inner dynein arms in situ in Chlamydomonas reinhardtii flagella. *J. Cell Biol.* **183**, 923–932 (2008).
12. Nicastro, D., Schwartz, C., Pierson, J., Gaudette, R., Porter, M.E. & McIntosh, J.R. The molecular architecture of axonemes revealed by cryoelectron tomography. *Science* **313**, 944–948 (2006).
13. Pigino, G., Maheshwari, A., Bui, K.H., Shingyoji, C., Kamimura, S. & Ishikawa, T. Comparative structural analysis of eukaryotic flagella and cilia from *Chlamydomonas*, *Tetrahymena*, and sea urchins. *J. Struct. Biol.* **178**, 199–206 (2012).
14. Ueno, H., Ishikawa,T., Bui, K.H., Gonda, K., Ishikawa, T. & Yamaguchi, T. Mouse respiratory cilia with the asymmetric axonemal structure on sparsely distributed ciliary cells can generate overall directional flow. *Nanomedicine* **8**, 1081–1087 (2012).
15. Kojima, H., Toba, S., Sakakibara, H. & Oiwa, K. Biophysical measurements on axonemal dyneins. *Methods Cell Biol.* **92**, 83–105 (2009).
16. Bui, K.H., Sakakibara, H., Movassagh, T., Oiwa, K. & Ishikawa, T. Asymmetry of inner dynein arms and inter-doublet links in Chlamydomonas flagella. *J. Cell Biol.* **186**, 437–446 (2009).
17. Bui, K.H., Yagi, T., Yamamoto, R., Kamiya, R. & Ishikawa, T. Polarity and asymmetry in the arrangement of dynein and related structures in the Chlamydomonas axoneme. *J. Cell Biol.* **198**, 913–925 (2012).
18. Hoops, H.J. & Witman, G.B. Outer doublet heterogeneity reveals structural polarity related to beat direction in Chlamydomonas flagella. *J. Cell Biol.* **97**, 902–908 (1983).
19. Omoto, C.K., Yagi, T., Kurimoto, E. & Kamiya, R. Ability of paralyzed flagella mutants of Chlamydomonas to move. *Cell Motil. Cytoskeleton* **33**, 88–94 (1996).
20. Kamiya, R. Functional diversity of axonemal dyneins as stud-

ied in Chlamydomonas mutants. *Int. Rev. Cytol.* **219**, 115–155 (2002).
21. Yagi, T., Minoura, I., Fujiwara, A., Saito, R., Yasunaga, T., Hirono, M. & Kamiya, R. An axonemal dynein particularly important for flagellar movement at high viscosity. Implications from a new Chlamydomonas mutant deficient in the dynein heavy chain gene DHC9. *J. Biol. Chem.* **280**, 41412–41420 (2005).
22. Yagi, T., Uematsu, K., Liu, Z. & Kamiya, R. Identification of dyneins that localize exclusively to the proximal portion of Chlamydomonas flagella. *J. Cell Sci.* **122**, 1306–1314 (2009).
23. Movassagh, T., Bui, K. H., Sakakibara, H., Oiwa, K. & Ishikawa, T. Nucleotide-induced global conformational changes of flagellar dynein arms revealed by in situ analysis. *Nat. Struct. Mol. Biol.* **17**, 761–767 (2010).
24. Shimizu, T., Marchese-Ragona, S. P. & Johnson, K. A. Activation of the dynein adenosinetriphosphatase by cross-linking to microtubules. *Biochemistry* **28**, 7016–7021 (1989).
25. Burgess, S. A., Walker, M. L., Sakakibara, H., Knight, P. J. & Oiwa, K. Dynein structure and power stroke. *Nature* **421**, 715–718 (2003).
26. Maheshwari, A. & Ishikawa, T. Heterogeneity of dynein structure implies coordinated suppression of dynein motor activity in the axoneme. *J. Struct. Biol.* **179**, 235–241 (2012).
27. Burgess, S. A. & Knight, P. J. Is the dynein motor a winch? *Curr. Opin. Struct. Biol.* **14**, 138–146 (2004).
28. Ueno, H., Yasunaga, T., Shingyoji, C. & Hirose, K. Dynein pulls microtubules without rotating its stalk. *Proc. Natl. Acad. Sci. USA* **105**, 19702–19707 (2008).
29. Omoto, C. K. & Brokaw, C. J. Bending patterns of Chlamydomonas flagella: II. Calcium effects on reactivated Chlamydomonas flagella. *Cell Motil.* **5**, 53–60 (1985).
30. Goodenough, U. W. & Heuser, J. E. Substructure of inner dynein arms, radial spokes, and the central pair/projection complex of cilia and flagella. *J. Cell Biol.* **100**, 2008–2018 (1985).
31. Yang, P., Diener, D. R., Yang, C., Kohno, T., Pazour, G. J., Dienes, J. M., Agrin, N. S., King, S. M., Sale, W. S., Kamiya, R., Rosenbaum, J. L. & Witman, G. B. Radial spoke proteins of Chlamydomonas flagella. *J. Cell Sci.* **119**, 1165–1174 (2006).
32. Pigino, G., Bui, K. H., Maheshwari, A., Lupetti, P., Diener, D. & Ishikawa, T. Cryoelectron tomography of radial spokes in cilia and flagella. *J. Cell Biol.* **195**, 673–687 (2011).
33. Li, X., Mooney, P., Zheng, S., Booth, C. R., Braunfeld, M. B., Gubbens, S., Agard, D. A. & Cheng, Y. Electron counting and beam-induced motion correction enable near-atomic-resolution single-particle cryo-EM. *Nat. Methods* **10**, 584–590 (2013).
34. Sigworth, F. J. A maximum-likelihood approach to single-particle image refinement. *J. Struct. Biol.* **122**, 328–339 (1998).